

CSA-Net: Channel-wise Spatially Autocorrelated Attention Networks

Nick Nikzad

Institute for Integrated and Intelligent Systems
Griffith University, Australia

n.nikzaddehaji@griffith.edu.au

Yongsheng Gao

Institute for Integrated and Intelligent Systems
Griffith University, Australia

yongsheng.gao@griffith.edu.au

Jun Zhou

Institute for Integrated and Intelligent Systems
Griffith University, Australia

jun.zhou@griffith.edu.au

Abstract

In recent years, convolutional neural networks (CNNs) with channel-wise feature refining mechanisms have brought noticeable benefits to modelling channel dependencies. However, current attention paradigms fail to infer an optimal channel descriptor capable of simultaneously exploiting statistical and spatial relationships among feature maps. In this paper, to overcome this shortcoming, we present a novel channel-wise spatially autocorrelated (CSA) attention mechanism. Inspired by geographical analysis, the proposed CSA exploits the spatial relationships between channels of feature maps to produce an effective channel descriptor. To the best of our knowledge, this is the first time that the concept of geographical spatial analysis is utilized in deep CNNs. The proposed CSA imposes negligible learning parameters and light computational overhead to the deep model, making it a powerful yet efficient attention module of choice. We validate the effectiveness of the proposed CSA networks (CSA-Nets) through extensive experiments and analysis on ImageNet, and MS COCO benchmark datasets for image classification, object detection, and instance segmentation. The experimental results demonstrate that CSA-Nets are able to consistently achieve competitive performance and superior generalization than several state-of-the-art attention-based CNNs over different benchmark tasks and datasets.

1. Introduction

Over the last decade, convolutional neural networks (CNNs) have shown outstanding performance on a variety of computer vision applications [14]. Inspired by the

biological process of the human visual system, they produce discriminative and representative features from raw input signals without any prior manipulation. In general, convolutional neural networks (CNNs) are constructed by stacking a series of convolution layers, non-linear activation and down-sampling functions. All these architectures are capable of effectively capturing hierarchical patterns along all the input channels. While most early researches [18, 47, 49, 56] mainly focused on improving the joint encoding of spatial and channel information, some works attempted to exploit and model information carried by inter-dependencies among channels. Methods like squeeze and excitation networks (SENet) [22], bottleneck attention module (BAM) [40], convolutional block attention module (CBAM) [55], global-and-local (GALA) [35], and dense-and-implicit attention network (DIANet) [26] adopt channel-wise gating mechanisms to learn nonlinear synergies between channels in order to re-calibrate the feature map.

Despite the advantage of existing attention mechanisms [22, 26, 35, 53, 55] in exploiting inter-channel relationships of the convolutional feature maps, they have a common property in using global pooling (max and/or average) to summarize information carried by every feature map. The global pooled information is not the optimal feature to infer accurate channel attention [41, 55]. As illustrated in Figure. 1, due to the data dependency of statistical pooling operators (e.g. global maximum or global average value), feature maps with similar statistical characteristics can represent distinctive spatial relationships.

This paper addresses the above issue by modelling CNNs' feature maps as entities of a geographical analysis system in which entities are characterized by their statisti-

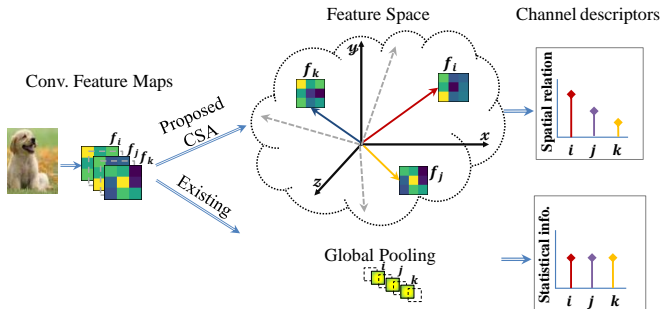


Figure 1. Conceptual comparison of the generic channel descriptors used by most of existing attention mechanisms [21, 22, 26, 35, 55] and the proposed one. Any image passing a convolutional layer is represented by a set of feature maps (Assume $f_i, f_j,$ and $f_k \in \mathbb{R}^3$). Due to the data dependency of statistical pooling operators, feature maps show similar statistical properties while their spatial relationships are distinctive.

cal and topological properties simultaneously. The “First Law of Geography” states that “everything is related to everything else, but near things are more related than distant things” [50]. For instance, people are less likely to travel greater distances to visit a store. Therefore, a retailer can determine the best possible locations for a new shop, considering how many people live within a 10-minute drive time from existing stores. Following this premise, the spatial inter-channel relationships of feature maps can tell us about the systematic spatial variation within feature maps, which is needed to address the aforementioned problem related to existing channel-wise attention modules. Here, we introduce Moran’s metric from geographical information science [37], for the first time, into the CNNs domain to analyse the geographical spatial correlation of the channel dependencies. We refer to the new attention unit, which adopts channel-wise spatial autocorrelation of deep feature maps as “channel-wise spatially autocorrelated” (CSA) attention block.

The overview of the proposed CSA framework is illustrated in Figure 2. To the best of our knowledge, this is the first time that the concept of geographical spatial analysis is utilized in deep CNNs. The implementation of the proposed CSA is straightforward and imposes negligible parameters overhead to the deep model. Furthermore, it can be easily integrated into baseline deep structures with negligible overhead to the computation cost. Therefore, our proposed CSA can be considered as a beneficial choice for other deep architectures as well.

The extensive experiments on image classification benchmark tasks show that the proposed channel-wise attention paradigm is able to effectively re-calibrate the feature maps by extracting inter-channel spatial dependencies. To verify the generalization capability of the proposed

CSA-Net, we demonstrate its effectiveness in object detection and instance segmentation. Further deep investigation studies are also conducted to investigate the characteristics of the proposed CSA.

2. Related Works

The critical role of a visual attention mechanism in human perception has been shown through a range of studies [11, 60]. The human vision system efficiently and adaptively focuses on salient areas and suppresses other irrelevant information. Attention mechanism has been widely incorporated in computer vision to improve the efficiency of the model [57, 58]. From the attention mechanism perspective, related works to this paper method can be divided into three main categories: First-order, Second-order and Self-attention techniques.

2.1. First-order methods

First-order statistics (*e.g.* global average pooling) have been widely used in most deep neural networks [17, 18, 25] to summarize the feature maps representation. Hu *et al.* [22] incorporated the global averaged statistics into a lightweight gating mechanism to exploit inter-channel relationships of the convolutional feature maps. Their squeeze-and-excitation (SE) module measures channel-wise attention by squeezing first-order spatial information. Nevertheless, SENets’ global squeezing function causes two main issues in producing a fine attention map: sub-optimal effect of global average-pooled features and missing spatial axes [40, 55]. Following the idea of attention mechanism in SENets, channel-wise attention (also known as feature-based attention) and spatial attention are two main streams to advance attention module in CNNs.

In this regard, the competitive SE (CMPE-SE) network [24] re-scales the value for each channel by modelling the competition between residual and identity mappings. On the other hand, the bottleneck attention module (BAM) [40] presents a 3D attention map that considers both channel and spatial axes simultaneously. Convolutional block attention module (CBAM) [55] introduces similar approaches to exploit spatial and channel-wise attention sequentially. Moreover, CBAM [55] uses global max-pooled features as an extra clue to infer a finer channel attention map. Global-and-local (GALA) [35] combines spatial- and feature-based attentions into a single mask that refines feature representations. The GALA module can be supervised by human feedback to learn what and where to attend. Similarly, batch aware attention module (BA²M) [10] fuses channel (based on the global average pooling), local spatial, and global spatial attention maps to obtain the sample-wise attention representation (SAR). These SARs are then normalised to derive weights for each sample, capturing varying feature importance across content complexities within

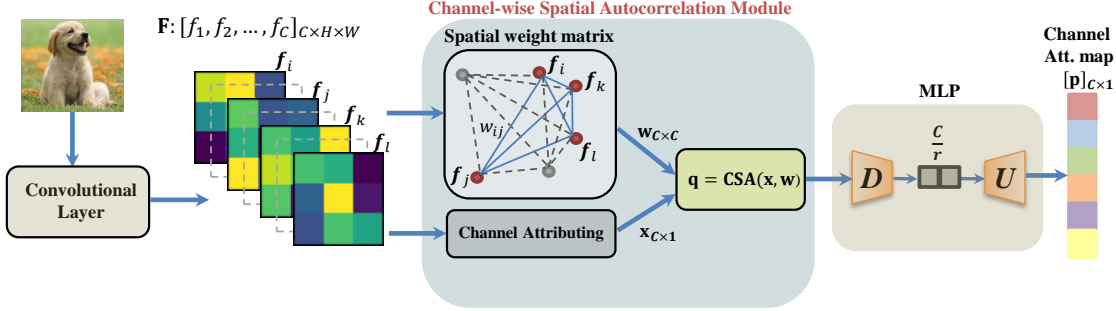


Figure 2. The proposed CSA framework for modelling channel-wise attention maps. As illustrated, spatial autocorrelation of feature maps is utilized to refine global contextual information. Boxes with different colours demonstrate different values of the computed attention map upon the channel axis. \mathbf{q} refers to the computed spatially autocorrelated channel descriptors. D and U indicate fully connected layers of the multi-layer perceptron (MLP) for channel reduction and up-sampling, respectively.

the batch.

Apart from these techniques, the bridge attention network (BA-Net) [62] integrates previous features into the attention layer using straightforward strategies similar to the SENets [23]. The top-down attention module (TDAM) [27] iteratively generates a “visual searchlight” that performs channel and spatial modulation on its inputs and outputs, resulting in more contextually-relevant feature maps at each computation step. The dense-and-implicit attention network (DIANet) [26] includes a densely connected framework that shares an attention module throughout the network. In particular, its attention mechanism incorporates Long Short-Term Memory (LSTM) [20], rather than fully connected layers in SENet [22], to capture long-distance channel-wise dependency. Wang *et al.* [53] developed an efficient channel attention (ECA) network to adaptively determine coverage of local cross-channel interaction in the excitation layer. On the other hand, Ruan *et al.* [45] proposed a parameter-free Gaussian context transformer (GCT), which replaced the fully-connected layers of the SE model and aimed to capture the presumed negative correlation between global contexts and attention activations [44]. Building upon GCT [45], Chen *et al.* [7] introduced the bilateral asymmetric skewed Gaussian attention (bi-SGA), which combines the skewed and asymmetric properties to further enhance the attention mechanism within GCT [45].

2.2. Second order methods

Higher-order statistics have shown the capability of modelling discriminative image representation [4, 15]. The global second-order squeezing methods benefit from covariance matrix representations of images to achieve performance improvement [16, 30, 31, 52]. Due to the high computation overhead of covariance matrix caused by the high resolution feature maps of the intermediate layers, these methods are mostly plugged at the deep network end. Though several attempts [4, 12, 13, 15] have tried to alle-

viate this issue by adopting compact covariance representations, they are only applicable at the deepest layers of deep networks.

In this regard, Gao *et al.* [16] proposed a global second-order pooling method, which introduces an effective feature aggregation method by considering the pairwise channel correlations of the input tensor. It also utilizes convolutions and non-linear activation to accomplish embedding of the resulting covariance matrix used for scaling the 3D tensor along the channel dimension. However, despite plugging the GSoP [16] into any layer of deep neural networks, the computation of the generated covariance matrix still imposes high computational costs (FLOPs) on the model. In this paper, unlike other covariance-based second-order approaches, we show that the proposed channel-wise spatial autocorrelation framework offers a more efficient and effective second-order attention mechanism.

2.3. Self-attention methods

The proposed method is also related to self-attention mechanisms [51, 59] from the perspective of modelling long-range dependencies across input feature maps. The self-attention module calculates response at a position in a sequence by weighting the sum of the features at all positions within the same sequence. In general, given the input sequence of a flattened tensor with the shape of $(C \times (HW))$ (C , H , and W represent the number of channels, height, and width of the input tensor), self-attention algorithms calculate the triplet (key, query, value). Then, the softmax-normalized dot-product of the query with all keys is computed to get the attention scores. Finally, the values are reweighted by the attention scores [2, 28, 42, 51].

In this regard, Bello *et al.* [2] proposed attention augmented (AA) convolutional network by combining convolutional and self-attention processing mechanisms. However, AA [2] still is not efficiently applicable throughout the

network including early high-resolution layers due to high memory and computational costs. To alleviate this shortcoming, Ramachandran *et al.* [42] introduced stand-alone self-attention (SASA) restricting the scope of self-attention to a local patch (e.g., 7×7 pixels), rather than applying global self-attention over a whole feature map [2, 51]. On top of this, Zhao *et al.* [61] explored two types of vector-based self-attention modules to replace all the spatial convolution layers in the common CNNs and yield the self-attention network (SAN) topology.

Despite the success of self-attention mechanisms for many applications, they suffer from a critical shortcoming of high computational costs, which makes them less practical to be efficiently incorporated with intermediate layers of a deep CNN processing relatively high-resolution feature maps [2, 28]. For instance, having a feature map $\mathbf{x} \in \mathbb{R}^{C \times 100 \times 100}$ (C represents the number of channels and $C \ll 100 \times 100$), a self-attention module generates a huge spatial attention map with the size of 10000×10000 to describe each pixel’s attention score on every other pixel. On the other hand, as discussed in [3, 54], self-attention can be also viewed as a form of the non-local mean and in this sense, some recent methods like gather-excitation (GE) [21], non-local spatial attention module (NL-SAM) [6], and global context network (GCNet) [5] effectively model the global spatial context using a non-local network (NLNet) [54], which at the same time introduces significant computational expense to the models.

3. Channel-wise Spatially Autocorrelated Attention Module

3.1. Geographical Spatial Auto-correlation

In this paper, we address the global contextual information squeezing problem of channel-wise attention mechanisms [22, 40, 55] from a geographical analysis perspective. To bridge the gap between the fields of CNNs and geographical analysis, we briefly review the concept of spatial autocorrelation in geographical science, which is needed to understand our work.

In geographical modelling, spatial autocorrelation plays an important role to measure spatial dependency of entities based on both entities’ locations and values simultaneously. Positive spatial autocorrelation indicates adjacent observations (entities) have similar values, while negative spatial autocorrelation means that nearby observations tend to have contrasting values. In general, there are two types of measures: global measures that summarize the level of spatial autocorrelation with respect to all data points and local measures that provide a value for each location concerning its neighbourhood. To calculate such measurements, Moran’s metric [37] is a technique that is used in geographical anal-

ysis. In this paper, to the best of our knowledge, for the first time, we use Moran’s measurement to investigate spatial dependency within deep feature maps. Moreover, as we aim at investigating the spatial properties of each feature map, we focus only on local Moran’s indicators [1].

Let \mathbf{F} be a set of C observations presented by location vectors f_i , $\mathbf{F} = [f_1, f_2, \dots, f_C]$, and an associated attribute, $\mathbf{x} = [x_1, x_2, \dots, x_C]$, the local Moran’s I metric can be defined as:

$$I_l(i) = \frac{C(x_i - \mu) \sum_{j=1}^C v_{ij}(x_j - \mu)}{\sum_{i=1}^C \sum_{j=1}^C v_{ij} \sum_{i=1}^C (x_i - \mu)^2} \quad (1)$$

where μ is the mean value of features upon their attribute. v_{ij} represents the elements of a spatial contiguity matrix $\mathbf{v} = [v_{ij}]_{C \times C}$, in which v_{ij} denotes the degree of closeness or the contiguous relationships between f_i and f_j ($i, j = 1, 2, \dots, C$). There are several ways to construct deterministic $\mathbf{v} = [v_{ij}]_{C \times C}$ [8, 9]. For the sake of simplicity and following [9], we adopt the negative exponential function in this work as:

$$v_{ij} = \begin{cases} \exp\left(\frac{-l_{ij}}{\bar{l}}\right), & \text{if } i \neq j \\ 0, & \text{if } i = j. \end{cases} \quad (2)$$

where l_{ij} ¹ refers to the distance between f_i and f_j , and \bar{l} is the average distance between any two elements.

3.2. Channel Attributing

As illustrated in Figure 2, we need to adopt the spatial analysis to our channel-wise attention models. This can be done by replacing the notations of observation and system in geographical context with the terms of feature maps and convolutional layer, respectively. In fact, given a convolutional layer (*i.e.* a system) generates a number of observations, which is represented by corresponding feature maps, $f \in \mathbb{R}^d$ lies in a d -dimensional vector space. Every feature map f is attributed with corresponding channel descriptors (*e.g.* global average value).

In this regard, suppose there is an intermediate feature map $\mathbf{F} = [f_1, f_2, \dots, f_C] \in \mathbb{R}^{C \times H \times W}$, which is associated with its channel-wise global context features descriptor $\mathbf{x} = [x_1, x_2, \dots, x_C] \in \mathbb{R}^{C \times 1}$ as:

$$\mathbf{x} = \left[x_i = \frac{1}{H \times W} \sum_{h=1}^H \sum_{w=1}^W f_i(h, w) \right]_{C \times 1}, \quad (3)$$

where C and (H, W) denote the channel number and spatial dimension of the feature map, \mathbf{F} , respectively. $f_i(h, w)$ represents the i -th channel feature value at position (h, w) . Please note that more sophisticated strategies

¹Although l_{ij} can take any form of distance measurements, it refers to L_2 distance between f_i and f_j throughout the paper.

or application-oriented criteria can be applied to obtain the global contextual information descriptor (Eq. (3)). Here, we use the global average pooling for the sake of simplicity.

3.3. Channel-wise Spatial Autocorrelation

As shown in [9], satisfying the further condition of unitary normalization enables a simpler and easier form of Eq.(1) for implementation. Therefore, following the technique proposed by Chen [9], the C -by- C unitary spatial weight matrix (USWM), \mathbf{w} , can be derived from Eq. (2) as:

$$\mathbf{w} = \left[w_{ij} = \frac{v_{ij}}{\sum_{i=1}^C \sum_{j=1}^C v_{ij}} \right]_{C \times C}, \sum_{i=1}^C \sum_{j=1}^C w_{ij} = 1 \quad (4)$$

Having the unitary spatial weight matrix, \mathbf{w} , Eq. (1) can be simplified as:

$$\mathbf{I}_l = [\text{diag}(\mathbf{z}^t \mathbf{z} \mathbf{w})]_{C \times 1}, \quad (5)$$

where $\text{diag}(\cdot)$ returns the diagonal elements of a matrix. \mathbf{z} refers to normalised channel-wise global context features as:

$$\mathbf{z} = \frac{\mathbf{x}^t - \mu}{\sigma}, \quad (6)$$

where μ and σ denote mean and standard deviation of \mathbf{x} , respectively. Symbol “ t ” indicates the transpose of the matrix.

Since the unitary spatial weights matrix (USWM), $\mathbf{w} = [w_{ij}]_{C \times C}$, is relatively big ($C \times C \geq 64 \times 64$), the normalization operation in Eq. (4) (i.e., $\frac{v_{ij}}{\sum_{i=1}^C \sum_{j=1}^C v_{ij}}$) leads to very small values of w_{ij} and consequently results in extremely small values in elements of \mathbf{I}_l (Eq. (5)). Such too small values in \mathbf{I}_l may exceed the precision of the floating point and be rounded to zero during computation. To avoid this issue, the channel-wise spatial autocorrelation descriptor, \mathbf{q} , can be defined as normalised \mathbf{I}_l :

$$\mathbf{q} = \frac{\mathbf{I}_l - \mu_{I_l}}{\sigma_{I_l}}, \quad (7)$$

where μ_{I_l} and σ_{I_l} indicate mean and standard deviation of \mathbf{I}_l , respectively.

3.4. Channel Attention Map

We construct spatially autocorrelated channel-wise gating mechanism by forming a multi-layer perceptron (MLP) with one hidden layer. The generated channel descriptor from previous step, \mathbf{q} , is forwarded to the MLP in which its first fully-connected (FC) layer followed by a non-linearity δ (ReLU [38]) reduces the channel dimension with ratio r (here, we set $r = 16$). Then an up-sampling FC layer followed by sigmoid activation, α , returns the input channel

dimension (C). So the channel attention map can be formalized as:

$$\mathbf{p} = \alpha(U(\delta(D(\mathbf{q})))), \quad (8)$$

where D and U represent the FC layers for channel reduction and up-sampling operators respectively.

3.5. Integration with Deep Networks

The proposed CSA framework can be easily integrated with deep architectures. The given output feature maps $\mathbf{F} \in \mathbb{R}^{C \times H \times W}$ of a convolutional unit is adaptively refined by the spatially autocorrelated channel-wise attention map, $\mathbf{p} \in \mathbb{R}^{C \times 1 \times 1}$. The overall process can be summarized as:

$$\mathbf{F} = \mathbf{p} \otimes \mathbf{F}, \quad (9)$$

where \otimes denotes element-wise multiplication. In this work, we integrate the CSA module into the final convolution layer within each resolution scale of the deep network.

3.6. Implementation Details

We use stochastic gradient descent (SGD) with a similar optimization configuration as [18] for the training of all models. In particular, we adopt Nesterov momentum [48] with a momentum weight of 0.9, and 10^{-4} as the weight decay.

On ImageNet, we train our models for 100 epochs with a mini-batch size of 128. For this experiment, the initial learning rate is set to 0.1 and is decreased by a factor of 10 at epochs 30, 60, and 90, respectively. For MS-COCO-2017 object detection and instance image segmentation tasks, models are trained for 24 epochs. All models are developed using PyTorch version 1.10 and trained on two NVIDIA GeForce V100 GPU cards with CUDA/cuDNN 11.0 toolkits.

4. Experimental Results and Discussion

The effectiveness of the proposed CSA model is evaluated across different deep architectures as well as different tasks. We use ImageNet-1K [14] for image classification. Further, MS-COCO-2017 [34] is utilized for object detection and instance segmentation tasks.

4.1. ImageNet Image Classification

In order to demonstrate CSA’s effectiveness on large-scale datasets and in a rigorous condition, we evaluate CSA with two baseline networks, *i.e.* ResNet-50 and ResNet-101 [17], and their attention-based variations on the ImageNet classification task [29]. ImageNet consists of 1.28 million images for training and 50,000 images for validation, respectively, from 1,000 classes. Following [17, 18],

Table 1. The top-1 and top-5 classification error rates (%) on ImageNet validation set. Single-crop validation errors are reported. Note that only channel-wise attention maps are used in the CBAM*’s attention mechanism [55]. The first and second best results are indicated in boldface and underlined-face, respectively.

Method	GFLOPs	Params.	top-1 err.	top-5 err.
ResNet-50 [17]	3.86	25.6M	24.70	7.80
+SE [22, 23]	3.87	28.1M	23.14	6.70
+CBAM* [55]	3.87	28.1M	22.80	6.52
+CBAM [55]	3.87	28.1M	22.66	6.32
+BAM [40]	3.94	25.9M	24.02	7.18
+GALA [35]	4.1	29.4M	22.73	6.35
+DIA [26]	-	28.4M	22.76	-
+NL-SAM [6]	7.03	32.5M	24.45	7.51
+AA [2]	8.30	25.8M	22.30	6.20
+SASA [42]	7.20	18.0M	22.40	-
+GSoP [16]	6.56	28.2M	22.49	6.24
+ECA [53]	4.13	25.5M	22.55	6.32
+FCA [41]	4.13	28.4M	21.43	5.90
+GCT [45]	4.12	25.6M	22.45	6.29
+BA-Net [62]	4.13	28.7M	21.15	5.72
+bi-SGA [7]	4.12	25.6M	22.36	6.3
+CSA (Ours)	4.12	26.2M	<u>21.41</u>	5.72
ResNet-101 [17]	7.58	44.5M	23.3	6.88
+SE [22, 23]	7.60	49.3M	22.35	6.19
+BAM [40]	7.65	49.9M	22.40	6.29
+AA [2]	16.10	45.4M	21.30	5.62
+GSoP [16]	12.12	48.9M	22.08	6.05
+ECA [53]	7.86	44.5M	21.35	5.66
+FCA [41]	7.86	49.3M	20.37	5.37
+GCT [45]	7.86	44.5M	21.15	5.59
+BA-Net [62]	7.87	50.5M	<u>20.97</u>	5.17
+bi-SGA [7]	7.86	44.5M	21.09	5.55
+CSA (Ours)	7.84	45.2M	<u>20.97</u>	<u>5.30</u>

we adopt similar data augmentation for training data alongside single-cropping of 224×224 . We also report classification error rates on the validation set. To the best of our knowledge, a few attention mechanisms [16, 41] have considered and tried to address the data dependency problem of global pooling. In addition to GSoP [16], Qin *et al.* [41] presented a frequency channel attention (FCA) mechanism which generalizes the squeezing of the channel attention mechanism in the frequency domain. Other methods either leverage spatial attention (it is not channel-wise) and max-pooling (BAM [40] and CBAM [55]), or focus on enhancing the excitation layer (GALA [35], NL-SAM [6], DIA [26], ECA [53], GCT [45], and bi-SGA [7]) to improve SE baseline, while they still use the same squeezing method as that of SENets [22, 23].

Table 1 shows the mean top-1 and top-5 classification error rates obtained by these models. It can be seen that networks equipped with the CSA module significantly outperform the ResNet-50 and ResNet-101 baselines and SE benchmarks. Moreover, the models with CSA outperform those counterparts that benefit from spatial resolution atten-

Table 2. Object detection mAP(%) on the MS-COCO 2017 validation set. ResNet-50 [17] is used as the backbone network for all models. The best results are indicated in boldface.

Method	mAP@[.5,.95]	mAP@.5	mAP@.75	mAP _S	mAP _M	mAP _L
Faster-RCNN [43]	36.4	58.2	39.2	21.8	40.0	46.2
+SE [23]	37.7	60.1	40.9	22.9	41.9	48.2
+AA [2]	39.4	61.0	42.3	-	-	-
+GSoP [16]	39.4	60.5	42.9	23.2	43.1	49.8
+ECA [53]	38.0	60.6	40.9	23.4	42.1	48.0
+FCA [41]	39.0	61.1	42.3	23.7	42.8	49.6
+GCT [45]	38.9	60.4	42.3	22.8	43.1	49.7
+BA-Net [62]	39.5	61.3	43.0	24.5	43.2	50.6
+bi-SGA [7]	39.2	60.5	42.5	23.2	43.1	49.8
+CSA (Ours)	39.7	61.1	43.1	23.4	43.5	51.3
Mask-RCNN [19]	37.2	58.9	40.3	22.2	40.7	48.0
+SE [23]	38.7	60.9	42.1	23.4	42.7	50.0
+GSoP [16]	39.9	60.4	43.5	23.7	42.9	52.3
+ECA [53]	39.0	61.3	42.1	24.2	42.8	49.9
+FCA [41]	40.3	62.0	44.1	25.2	43.9	52.0
+GCT [45]	39.4	60.8	42.9	23.6	43.3	50.7
+BA-Net [62]	40.5	61.7	44.2	24.5	44.3	52.1
+bi-SGA [7]	38.6	61.0	43.0	23.6	43.5	50.8
+CSA (Ours)	40.5	61.6	44.4	24.3	44.1	53.0

tion map (BAM [40], CBAM [55], GALA [35]). These results demonstrate the effectiveness of the proposed spatial autocorrelation analysis of feature maps in generating richer channel descriptors.

The CSA also achieves lower error rates than the second order method GSoP [16] and the non-local/self-attention methods NL-SAM [6], AA [2], and SASA [42] with about half computational expense (GFLOPs). The result shows the effectiveness and yet the efficiency of CSA against benchmarks. Though CSA obtains competitive performance against FCA [41] and BA-Net [62], our further evaluations on object detection (see Table 2) and instance segmentation (see Table 3) tasks reveal that the CSA shows superior generalization ability on the three different tasks.

4.2. MS-COCO Object Detection

In addition to the image classification task, we also use the Microsoft (MS)-COCO 2017 dataset [33] to evaluate the generalization capability of the proposed CSA module on object detection tasks. MS-COCO is a large-scale object detection, segmentation, key-point detection, and captioning dataset. In this work, we conduct object detection on this dataset. Microsoft-COCO dataset splits into two sets of 115K (“2017 train”) and 5K (“2017 val”) images for training and validating purposes, respectively. Following [41, 53], and [23], we adopt Faster-RCNN [43] and Mask-RCNN [19] as the detection models and ImageNet pre-trained ResNet-50 as the backbone network. Here, following [23], we plug CSA into base architecture to evaluate its benefit. The MS-COCO’s standard evaluation metric mAP over different IoU with thresholds from 0.5 to 0.95 as well as mAP on small (mAP_S), medium-size (mAP_M) and large (mAP_L) ground truth objects are reported, respectively. We use SE [23], AA [2], GSoP [16], ECA [53], FCA [41], GCT [45], BA-Net [62], and bi-SGA [7] for

Table 3. Instance segmentation mAP(%) using Mask-RCNN [19] on the MS-COCO 2017 validation set. ResNet-50 [17] is used as the backbone network for all models. The best results are indicated in boldface.

Method	mAP@[.5,.95]	mAP@.5	mAP@.75
Mask-RCNN [19]	34.1	55.5	36.2
+SE [23]	35.4	57.4	37.8
+GSoP [16]	36.0	57.5	38.2
+ECA [53]	35.6	58.1	37.7
+FCA [41]	36.2	58.6	38.6
+GCT [45]	35.7	57.6	38.0
+BA-Net [62]	36.6	58.7	38.6
+bi-SGA [7]	35.9	57.6	38.1
+CSA (Ours)	36.5	58.8	38.8

Table 4. Comparison of the training and inference time per batch between the baseline ResNet-50, the proposed CSA model and the SE [23] counterpart integrated into a ResNet-50 network and trained on ImageNet. All methods’ input resolution and batch size are 224×224 and 128, respectively.

Method	training time	inference time	top-1 err.
ResNet-50 [17]	0.134s	0.133s	24.70
+SE [23]	0.426s	0.290s	23.14
+CSA (Ours)	0.508s	0.281s	21.36

comparison. As shown in Table 2, CSA can outperform its counterparts on most evaluation metrics demonstrating the generalization ability of the proposed CSA module on different tasks.

4.3. MS-COCO Instance Segmentation

We further conduct experiments on the instance segmentation task. In particular, we present instance segmentation results of our CSA module using Mask R-CNN on MS-COCO 2017. The standard evaluation metric mAP with the threshold from 0.5 to 0.95 is reported in Table 3. The results show that superior performance of the proposed CSA can be achieved for most of the different settings.

4.4. Analysis and Discussion

4.4.1 Computational Expense

Involving more computation is the inevitable cost of adopting channel-wise spatially autocorrelated attention units. Table 4 compares the time efficiency between the baseline ResNet-50, the proposed CSA model and the SE counterpart integrated into a ResNet-50 network. Under common settings for vision applications, utilising the ResNet-50 architecture and a batch size of 128 with input images at a resolution of 224×224 , the CSA exhibits marginal increments in training time per batch—specifically, an increase of 0.082s. Notably, the proposed CSA shows a slightly

quicker inference time compared to the SE method.

4.4.2 Spatially Autocorrelated Channel Descriptor

Though the effectiveness of the proposed CSA module has been proved empirically, we make a deeper investigation to provide a better understanding of its behaviour. To this end, we examine the relationship between the channel-wise global context (z), channel-wise spatial autocorrelation (q) and the corresponding channel attention map (p). In particular, we develop two distinct models by incorporating SE [23], and the proposed CSA attention modules into the ResNet-50 network. These models are subsequently trained on the ImageNet dataset. Then, we compute and analyse the averaged global context, averaged spatial autocorrelation features and corresponding attention values across the 1000 classes in the ImageNet validation set. Please note that the calculation of spatial autocorrelation measure does not involve any learnable parameters. Therefore, it is applicable to and can be computed for other trained networks such as the SE model as well.

Figure 5 illustrates the results from the last convolutional layer at all resolution scales of ResNet-50. The averaged spatial autocorrelation features are sorted in ascending order to facilitate the observation. As shown in [36, 63], low-level features are generated at the early stages. Notably, our CSA attention module maintains a nearly uniform attention distribution among channels for the first resolution scale, indicating that it preserves all the extracted low-level features generated at the early stage. This approach differs from SE, which prioritises channels based on their global contextual values.

In scales two and three, our proposed CSA shows a positive correlation between spatial autocorrelation and attention values. This implies CSA’s capability to leverage spatial dependency in intermediate stages of deep networks, giving higher attention to features with higher spatial autocorrelation for the process of subsequent scales. Similar trends are observed in SE, however, with a weaker positive correlation at scale three.

Figure 5 reveals an interesting trend among two models in the last scale, where the spatial autocorrelation among their feature maps tends to be lower, indicating reduced spatial correlation during the generation of final features. Notably, the proposed CSA method demonstrates the lowest channel-wise spatial autocorrelation, approaching zero for most channels. This suggests that CSA’s final features are almost spatially uncorrelated, which proves by [32, 39] to be more discriminative features.

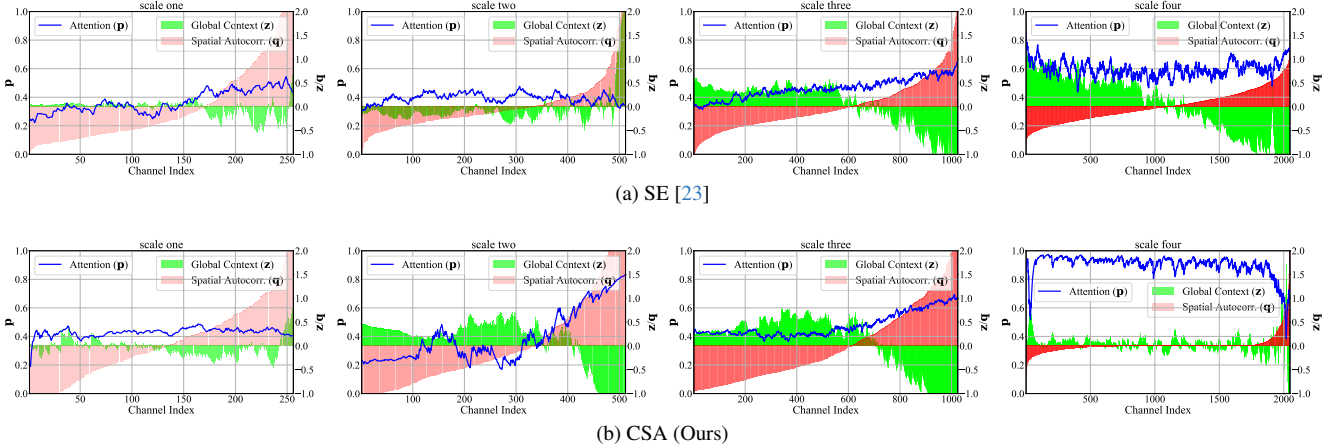


Figure 3. Visualising the relationship between averaged channel-wise global context (z), channel-wise spatial autocorrelation (q), and corresponding channel attention map (p) produced by the proposed CSA and SE [23] attention mechanisms in the last convolutional block at each resolution scale of ResNet-50 on the ImageNet validation set. Please note: the attention values for SE [23] are based on their global average pooling, while the proposed CSA is based on channels’ spatial autocorrelation. For better presentation, the graphs are smoothed by the exponential moving average with a factor of 0.3.

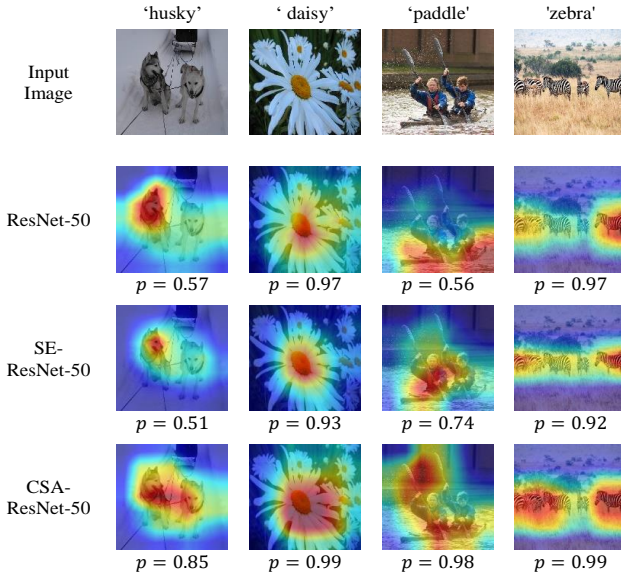


Figure 4. Visual comparisons of Grad-CAM [46] analysis generated by the last convolutional outputs layer in ResNet-50, SE-ResNet-50 [23], and CSA-ResNet-50 (Ours) on ImageNet. The target class label is shown on the top of each input image, and p indicates the probability score of each model for the target class.

4.4.3 Network Visualization

Besides analyzing the above-mentioned characteristics of the spatially autocorrelated channel descriptor, we investigate the effectiveness of the proposed CSA from another perspective. For this purpose, we apply the Gradient-weighted Class Activation Mapping (Grad-CAM) [46] to

qualitatively analyze different networks using the ImageNet validation set. Grad-CAM is a class-discriminative localization technique generally used to visualize particular parts of the image that influence the whole model’s decision for an assigned class label. In particular, it uses the gradients of any target concept with respect to the latest activation map to produce a coarse localization map highlighting the crucial regions in the image for predicting the concept [46]. As shown in [46], observing the crucial areas that the network considers for predicting a class provides us with a qualitative visual intuition of how the model performs in the effective use of features.

Figure 6 illustrates the visualization comparison of the Grad-CAM masks generated by the proposed CSA and SE attention modules integrated with the baseline ResNet-50. It can be seen that the CSA network’s results cover the class-discriminative regions better than other methods, which demonstrates its superior ability in aggregating features and exploiting information from the target object. Moreover, CSA network produces the highest target classes’ probability scores.

5. Conclusion

In this paper, we present a novel channel-wise spatially autocorrelated (CSA) attention module. For the first time, with the light of geographical spatial analysis, CSA utilizes an effective spatial autocorrelation schema to efficiently exploit spatial inter-dependencies among channels of feature maps. This property enables the CSA-Nets to improve the representational capacity of the network by adaptively recalibrating channel-wise spatially autocorrelated features.

Our extensive experiments verify that the CSA-Nets are able to present a better performance compared to recently advanced attention paradigms.

Apart from the demonstrated novelty and effectiveness of the proposed method, several directions can be considered as future works. One possibility is enhancing the CSA attention module with parametric embedding methods to effectively and yet efficiently model spatial contiguity matrix and feature correlations. Another possible prospective study can be investigating the CSA’s potential as a channel descriptor for other attention mechanisms and applications beyond its current scope. For instance, it could be evaluated as a replacement for conventional global average pooling, unlocking new possibilities for attention-based schemes.

References

- [1] Luc Anselin. Local indicators of spatial association—LISA. *Geographical analysis*, 27(2):93–115, 1995. 4
- [2] Irwan Bello, Barret Zoph, Ashish Vaswani, Jonathon Shlens, and Quoc V Le. Attention augmented convolutional networks. In *ICCV*, pages 3286–3295, 2019. 3, 4, 6
- [3] Antoni Buades, Bartomeu Coll, and J-M Morel. A non-local algorithm for image denoising. In *CVPR*, pages 60–65. IEEE, 2005. 4
- [4] Sijia Cai, Wangmeng Zuo, and Lei Zhang. Higher-order integration of hierarchical convolutional activations for fine-grained visual categorization. In *ICCV*, pages 511–520, 2017. 3
- [5] Yue Cao, Jiarui Xu, Stephen Lin, Fangyun Wei, and Han Hu. GCNet: Non-local networks meet squeeze-excitation networks and beyond. In *ICCV Workshops*, pages 0–0, 2019. 4
- [6] Bingling Chen, Yan Huang, Qiaoqiao Xia, and Qinglin Zhang. Nonlocal spatial attention module for image classification. *International Journal of Advanced Robotic Systems*, 17(5):1729881420938927, 2020. 4, 6
- [7] Cheng Chen and Bo Li. An interpretable channelwise attention mechanism based on asymmetric and skewed gaussian distribution. *Pattern Recognition*, 139:109467, 2023. 3, 6, 7
- [8] Yanguang Chen. On the four types of weight functions for spatial contiguity matrix. *Letters in Spatial and Resource Sciences*, 5(2):65–72, 2012. 4
- [9] Yanguang Chen. New approaches for calculating Moran’s index of spatial autocorrelation. *PloS one*, 8(7), 2013. 4, 5
- [10] Qishang Cheng, Hongliang Li, Qingbo Wu, and King Ngi Ngan. BA²M: A batch aware attention module for image classification. *arXiv preprint arXiv:2103.15099*, 2021. 2
- [11] Maurizio Corbetta and Gordon L Shulman. Control of goal-directed and stimulus-driven attention in the brain. *Nature reviews neuroscience*, 3(3):201–215, 2002. 2
- [12] Yin Cui, Feng Zhou, Jiang Wang, Xiao Liu, Yuanqing Lin, and Serge Belongie. Kernel pooling for convolutional neural networks. In *CVPR*, pages 2921–2930, 2017. 3
- [13] Xiyang Dai, Joe Yue-Hei Ng, and Larry S Davis. FASON: First and second order information fusion network for texture recognition. In *CVPR*, pages 7352–7360, 2017. 3
- [14] Jia Deng, Wei Dong, Richard Socher, Li-Jia Li, Kai Li, and Li Fei-Fei. ImageNet: A large-scale hierarchical image database. In *CVPR*, pages 248–255. IEEE, 2009. 1, 5
- [15] Yang Gao, Oscar Beijbom, Ning Zhang, and Trevor Darrell. Compact bilinear pooling. In *CVPR*, pages 317–326, 2016. 3
- [16] Zilin Gao, Jiangtao Xie, Qilong Wang, and Peihua Li. Global second-order pooling convolutional networks. In *CVPR*, pages 3024–3033, 2019. 3, 6, 7
- [17] Kaiming He, Xiangyu Zhang, Shaoqing Ren, and Jian Sun. Deep residual learning for image recognition. In *CVPR*, pages 770–778, 2016. 2, 5, 6, 7
- [18] Kaiming He, Xiangyu Zhang, Shaoqing Ren, and Jian Sun. Identity mappings in deep residual networks. In *ECCV*, pages 630–645. Springer, 2016. 1, 2, 5
- [19] Kaiming He, Georgia Gkioxari, Piotr Dollár, and Ross Girshick. Mask R-CNN. In *ICCV*, pages 2961–2969, 2017. 6, 7
- [20] Sepp Hochreiter and Jürgen Schmidhuber. Long short-term memory. *Neural computation*, 9(8):1735–1780, 1997. 3
- [21] Jie Hu, Li Shen, Samuel Albanie, Gang Sun, and Andrea Vedaldi. Gather-excite: Exploiting feature context in convolutional neural networks. In *NeurIPS*, pages 9401–9411, 2018. 2, 4
- [22] Jie Hu, Li Shen, and Gang Sun. Squeeze-and-excitation networks. In *CVPR*, pages 7132–7141, 2018. 1, 2, 3, 4, 6
- [23] J. Hu, L. Shen, S. Albanie, G. Sun, and E. Wu. Squeeze-and-excitation networks. *IEEE Transactions on Pattern Analysis and Machine Intelligence*, 42(8):2011–2023, 2020. 3, 6, 7, 8, 1, 2
- [24] Yang Hu, Guihua Wen, Mingnan Luo, Dan Dai, Jia-jiong Ma, and Zhiwen Yu. Competitive inner-imaging squeeze and excitation for residual network. *arXiv preprint arXiv:1807.08920*, 2018. 2
- [25] Gao Huang, Zhuang Liu, Laurens Van Der Maaten, and Kilian Q Weinberger. Densely connected convolutional networks. In *CVPR*, page 3, 2017. 2
- [26] Zhongzhan Huang, Senwei Liang, Mingfu Liang, and Haizhao Yang. DIANet: Dense-and-implicit attention network. In *AAAI*, pages 4206–4214, 2020. 1, 2, 3, 6
- [27] Shantanu Jaiswal, Basura Fernando, and Cheston Tan. TDAM: Top-down attention module for contextually guided feature selection in cnns. In *ECCV*, pages 259–276. Springer, 2022. 3
- [28] Salman Khan, Muzammal Naseer, Munawar Hayat, Syed Waqas Zamir, Fahad Shahbaz Khan, and Mubarak Shah. Transformers in vision: A survey. *ACM Computing Surveys (CSUR)*, 2021. 3, 4
- [29] Alex Krizhevsky, Ilya Sutskever, and Geoffrey E Hinton. Imagenet classification with deep convolutional neural networks. In *NeurIPS*, pages 1097–1105, 2012. 5
- [30] Peihua Li, Jiangtao Xie, Qilong Wang, and Wangmeng Zuo. Is second-order information helpful for large-scale visual recognition? In *ICCV*, pages 2070–2078, 2017. 3
- [31] Peihua Li, Jiangtao Xie, Qilong Wang, and Zilin Gao. Towards faster training of global covariance pooling networks by iterative matrix square root normalization. In *CVPR*, pages 947–955, 2018. 3

- [32] Xuelong Li, Han Zhang, Rui Zhang, and Feiping Nie. Discriminative and uncorrelated feature selection with constrained spectral analysis in unsupervised learning. *IEEE Transactions on Image Processing*, 29:2139–2149, 2019. [7](#), [1](#)
- [33] Tsung-Yi Lin, Michael Maire, Serge J. Belongie, Lubomir D. Bourdev, Ross B. Girshick, James Hays, Pietro Perona, Deva Ramanan, Piotr Dollár, and C. Lawrence Zitnick. Microsoft COCO: common objects in context. *CoRR*, abs/1405.0312, 2014. [6](#)
- [34] Tsung-Yi Lin, Michael Maire, Serge Belongie, James Hays, Pietro Perona, Deva Ramanan, Piotr Dollár, and C Lawrence Zitnick. Microsoft COCO: Common objects in context. In *ECCV*, pages 740–755. Springer, 2014. [5](#)
- [35] Drew Linsley, Dan Shiebler, Sven Eberhardt, and Thomas Serre. Learning what and where to attend. In *ICLR*, 2019. [1](#), [2](#), [6](#)
- [36] Christoph Molnar. *Interpretable machine learning*. Lulu.com, 2020. [7](#), [1](#)
- [37] Patrick AP Moran. The interpretation of statistical maps. *Journal of the Royal Statistical Society. Series B (Methodological)*, 10(2):243–251, 1948. [2](#), [4](#)
- [38] Vinod Nair and Geoffrey E Hinton. Rectified linear units improve restricted Boltzmann machines. In *ICML*, pages 807–814, 2010. [5](#)
- [39] Feiping Nie, Xiaoqian Wang, and Heng Huang. Clustering and projected clustering with adaptive neighbors. In *ACM SIGKDD*, pages 977–986, 2014. [7](#), [1](#)
- [40] Jongchan Park, Sanghyun Woo, Joon-Young Lee, and In So Kweon. BAM: Bottleneck attention module. In *BMVC*, pages 1–14, 2018. [1](#), [2](#), [4](#), [6](#)
- [41] Zequn Qin, Pengyi Zhang, Fei Wu, and Xi Li. FCANET: Frequency channel attention networks. In *ICCV*, pages 783–792, 2021. [1](#), [6](#), [7](#)
- [42] Prajit Ramachandran, Niki Parmar, Ashish Vaswani, Irwan Bello, Anselm Levskaya, and Jon Shlens. Stand-alone self-attention in vision models. In *NeurIPS*, 2019. [3](#), [4](#), [6](#)
- [43] Shaoqing Ren, Kaiming He, Ross Girshick, and Jian Sun. Faster-RCNN: Towards real-time object detection with region proposal networks. In *NeurIPS*, pages 91–99, 2015. [6](#)
- [44] Dongsheng Ruan, Jun Wen, Nenggan Zheng, and Min Zheng. Linear context transform block. In *AAAI*, pages 5553–5560, 2020. [3](#)
- [45] Dongsheng Ruan, Daiyin Wang, Yuan Zheng, Nenggan Zheng, and Min Zheng. Gaussian context transformer. In *CVPR*, pages 15129–15138, 2021. [3](#), [6](#), [7](#)
- [46] Ramprasaath R Selvaraju, Michael Cogswell, Abhishek Das, Ramakrishna Vedantam, Devi Parikh, and Dhruv Batra. Grad-CAM: Visual explanations from deep networks via gradient-based localization. In *ICCV*, pages 618–626, 2017. [8](#), [1](#), [3](#)
- [47] Karen Simonyan and Andrew Zisserman. Very deep convolutional networks for large-scale image recognition. In *ICLR*, 2015. [1](#)
- [48] Ilya Sutskever, James Martens, George Dahl, and Geoffrey Hinton. On the importance of initialization and momentum in deep learning. In *ICML*, pages 1139–1147, 2013. [5](#)
- [49] Christian Szegedy, Wei Liu, Yangqing Jia, Pierre Sermanet, Scott Reed, Dragomir Anguelov, Dumitru Erhan, Vincent Vanhoucke, and Andrew Rabinovich. Going deeper with convolutions. In *CVPR*, pages 1–9, 2015. [1](#)
- [50] Waldo R Tobler. A computer movie simulating urban growth in the detroit region. *Economic Geography*, 46(sup1):234–240, 1970. [2](#)
- [51] Ashish Vaswani, Noam Shazeer, Niki Parmar, Jakob Uszkoreit, Llion Jones, Aidan N Gomez, Łukasz Kaiser, and Illia Polosukhin. Attention is all you need. In *NeurIPS*, 2017. [3](#), [4](#)
- [52] Hao Wang, Qilong Wang, Mingqi Gao, Peihua Li, and Wangmeng Zuo. Multi-scale location-aware kernel representation for object detection. In *CVPR*, pages 1248–1257, 2018. [3](#)
- [53] Qilong Wang, Banggu Wu, Pengfei Zhu, Peihua Li, Wangmeng Zuo, and Qinghua Hu. ECA-Net: Efficient channel attention for deep convolutional neural networks. In *CVPR*, 2020. [1](#), [3](#), [6](#), [7](#)
- [54] Xiaolong Wang, Ross Girshick, Abhinav Gupta, and Kaiming He. Non-local neural networks. In *CVPR*, pages 7794–7803, 2018. [4](#)
- [55] Sanghyun Woo, Jongchan Park, Joon-Young Lee, and In So Kweon. CBAM: Convolutional block attention module. In *ECCV*, pages 3–19, 2018. [1](#), [2](#), [4](#), [6](#)
- [56] Saining Xie, Ross Girshick, Piotr Dollár, Zhuowen Tu, and Kaiming He. Aggregated residual transformations for deep neural networks. In *CVPR*, pages 5987–5995. IEEE, 2017. [1](#)
- [57] Kelvin Xu, Jimmy Ba, Ryan Kiros, Kyunghyun Cho, Aaron Courville, Ruslan Salakhudinov, Rich Zemel, and Yoshua Bengio. Show, attend and tell: Neural image caption generation with visual attention. In *ICML*, pages 2048–2057, 2015. [2](#)
- [58] Shivanthan Yohanandan, Andy Song, Adrian G Dyer, and Dacheng Tao. Saliency preservation in low-resolution grayscale images. In *ECCV*, pages 235–251, 2018. [2](#)
- [59] Han Zhang, Ian Goodfellow, Dimitris Metaxas, and Augustus Odena. Self-attention generative adversarial networks. In *ICML*, pages 7354–7363. PMLR, 2019. [3](#)
- [60] Xian Zhang, Jason C Park, Jennifer Salant, Sonya Thomas, Joy Hirsch, and Donald C Hood. A multiplicative model for spatial interaction in the human visual cortex. *Journal of Vision*, 8(8):4–4, 2008. [2](#)
- [61] Hengshuang Zhao, Jiaya Jia, and Vladlen Koltun. Exploring self-attention for image recognition. In *CVPR*, pages 10076–10085, 2020. [4](#)
- [62] Yue Zhao, Junzhou Chen, Zirui Zhang, and Ronghui Zhang. BA-Net: Bridge attention for deep convolutional neural networks. In *ECCV*, pages 297–312. Springer, 2022. [3](#), [6](#), [7](#)
- [63] Bolei Zhou, David Bau, Aude Oliva, and Antonio Torralba. Interpreting deep visual representations via network dissection. *IEEE Transactions on Pattern Analysis and Machine Intelligence*, 41(9):2131–2145, 2018. [7](#), [1](#)

CSA-Net: Channel-wise Spatially Autocorrelated Attention Networks

Supplementary Material

6. Introduction

Due to the page limit in the main text, we provide high-resolution graphs for Subsection 4.4.2 (refer to Figure 3 in the main text) and additional Grad-Cam [46] visual comparisons for Subsection 4.4.3 (refer to Figure 4 in the main text) in the following sections. To maintain context between the main text and the provided figures, we reiterate the relevant text here as well.

7. Spatially Autocorrelated Channel Descriptor

Though the effectiveness of the proposed CSA module has been proved empirically, we make a deeper investigation to provide a better understanding of its behaviour. To this end, we examine the relationship between the channel-wise global context (\mathbf{z}), channel-wise spatial autocorrelation (\mathbf{q}) and the corresponding channel attention map (\mathbf{p}). In particular, we develop two distinct models by incorporating SE [23], and the proposed CSA attention modules into the ResNet-50 network. These models are subsequently trained on the ImageNet dataset. Then, we compute and analyse the averaged global context, averaged spatial autocorrelation features and corresponding attention values across the 1000 classes in the ImageNet validation set. Please note that the calculation of spatial autocorrelation measure does not involve any learnable parameters. Therefore, it is applicable to and can be computed for other trained networks such as the SE model as well.

Figure 5 illustrates the results from the last convolutional layer at all resolution scales of ResNet-50. The averaged spatial autocorrelation features are sorted in ascending order to facilitate the observation. As shown in [36, 63], low-level features are generated at the early stages. Notably, our CSA attention module maintains a nearly uniform attention distribution among channels for the first resolution scale, indicating that it preserves all the extracted low-level features generated at the early stage. This approach differs from SE, which prioritises channels based on their global contextual values.

In scales two and three, our proposed CSA shows a positive correlation between spatial autocorrelation and attention values. This implies CSA’s capability to leverage spatial dependency in intermediate stages of deep networks, giving higher attention to features with higher spatial autocorrelation for the process of subsequent scales. Similar

trends are observed in SE, however, with a weaker positive correlation at scale three.

Figure 5 reveals an interesting trend among two models in the last scale, where the spatial autocorrelation among their feature maps tends to be lower, indicating reduced spatial correlation during the generation of final features. Notably, the proposed CSA method demonstrates the lowest channel-wise spatial autocorrelation, approaching zero for most channels. This suggests that CSA’s final features are almost spatially uncorrelated, which proves by [32, 39] to be more discriminative features.

8. Network Visualization

Besides analyzing the above-mentioned characteristics of the spatially autocorrelated channel descriptor, we investigate the effectiveness of the proposed CSA from another perspective. For this purpose, we apply the Gradient-weighted Class Activation Mapping (Grad-CAM) [46] to qualitatively analyze different networks using the ImageNet validation set. Grad-CAM is a class-discriminative localization technique generally used to visualize particular parts of the image that influence the whole model’s decision for an assigned class label. In particular, it uses the gradients of any target concept with respect to the latest activation map to produce a coarse localization map highlighting the crucial regions in the image for predicting the concept [46]. As shown in [46], observing the crucial areas that the network considers for predicting a class provides us with a qualitative visual intuition of how the model performs in the effective use of features.

Figure 6 illustrates the visualization comparison of the Grad-CAM masks generated by the proposed CSA and SE attention modules integrated with the baseline ResNet-50. It can be seen that the CSA network’s results cover the class-discriminative regions better than other methods, which demonstrates its superior ability in aggregating features and exploiting information from the target object. Moreover, CSA network produces the highest target classes’ probability scores.

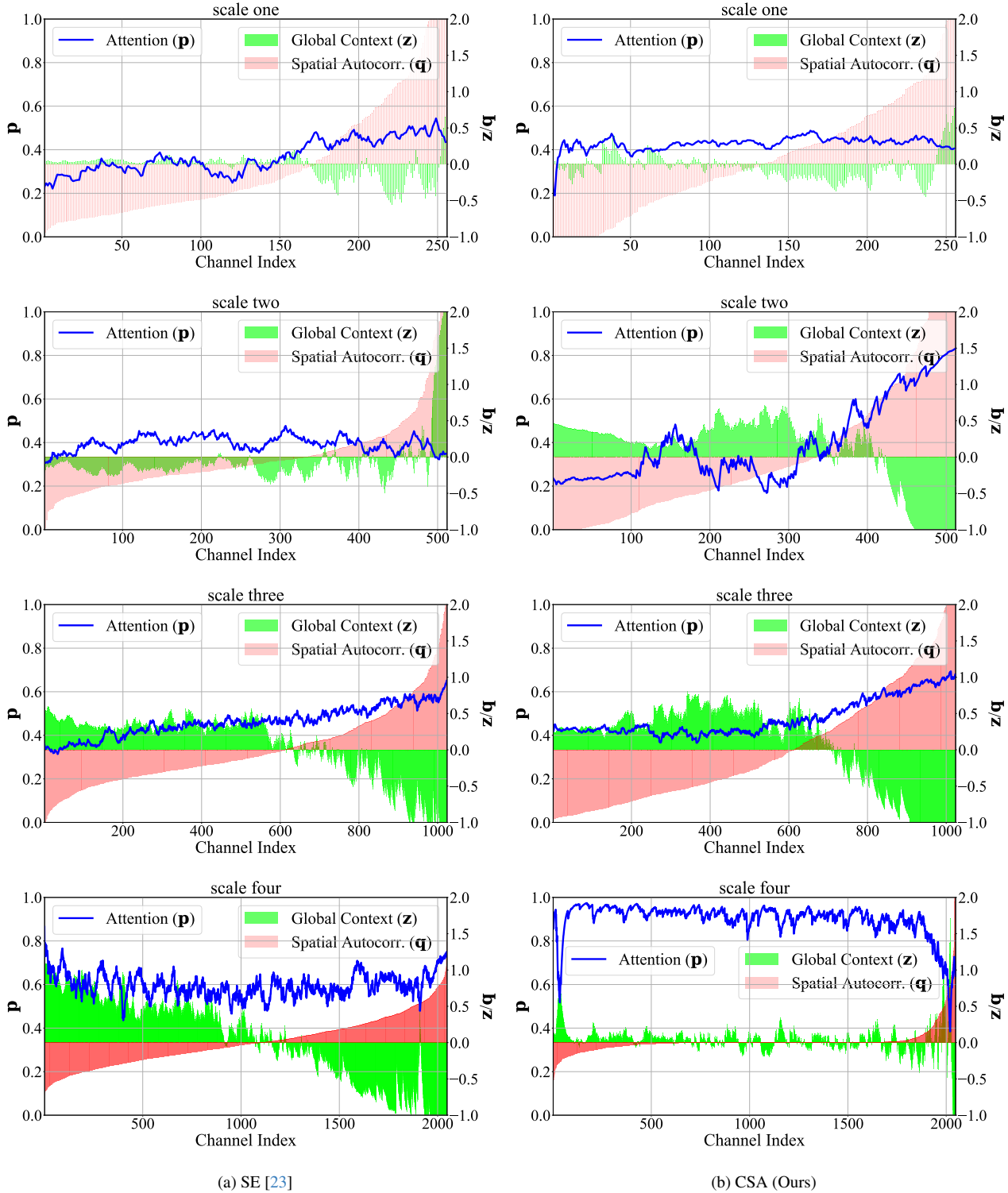


Figure 5. Visualising the relationship between averaged channel-wise global context (\mathbf{z}), channel-wise spatial autocorrelation (\mathbf{q}), and corresponding channel attention map (\mathbf{p}) produced by the proposed CSA and SE [23] attention mechanisms in the last convolutional block at each resolution scale of ResNet-50 on the ImageNet validation set. Please note: the attention values for SE [23] are based on their global average pooling, while the proposed CSA is based on channels’ spatial autocorrelation. For better presentation, the graphs are smoothed by the exponential moving average with a factor of 0.3.

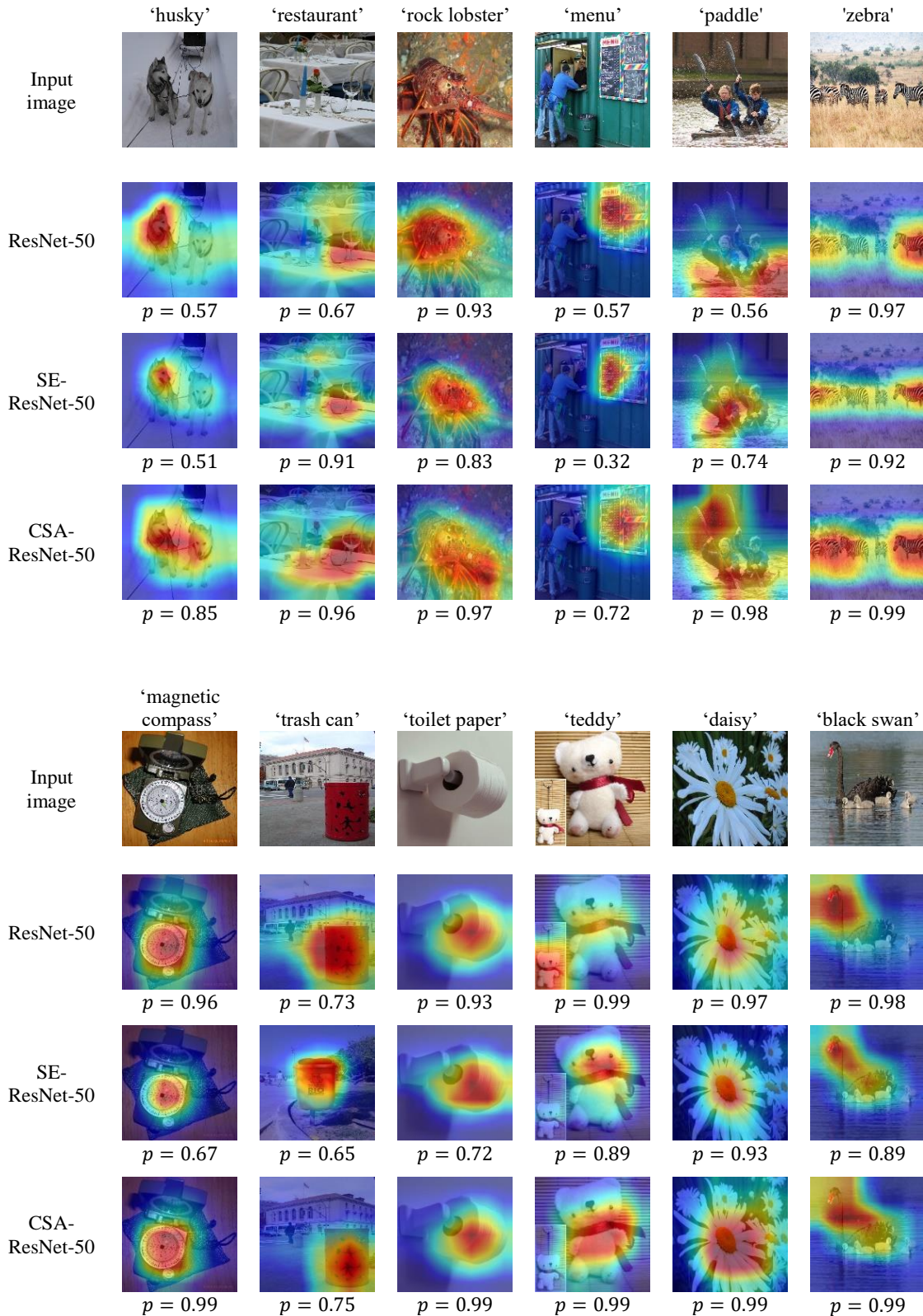


Figure 6. Visual comparisons of Grad-CAM [46] analysis generated by the last convolutional outputs layer in ResNet-50, SE-ResNet-50 [23], and CSA-ResNet-50 (Ours) on ImageNet. The target class label is shown on the top of each input image, and p indicates the probability score of each model for the target class.